Ice Classification in the Southern Ocean Using ERS-1 Scatterometer Data

David S. Early, David G. Long

Electrical and Computer Engineering Department, Brigham Young University
459 Clyde Building, Provo, Utah 84602
(801) 378-4383 fax: (801) 378-6586 long@ee.byu.edu

Abstract - **A simple method for classifying Southern Ocean sea ice from enhanced resolution ERS-1 scatterometer images is presented. The enhanced resolution images are created with the Scatterometer Image Reconstruction (SIR) algorithm. This algorithm uses a dense, irregular sample grid created with multiple, overlapping passes of the ERS-1 scatterometer to achieve resolutions better than the nominal 50 km ERS-1 resolution. Because the scatterometer provides measurements over a range of incidence angles, the incidence angle dependence of the observed σ^o can be used as part of the classification algorithm along with the incidence angle normalized σ^o, improving the accuracy of the classification. In this study, a third parameter, the standard deviation of a measure of the anisotropy, is used to further help delineate sea ice types.**

I. INTRODUCTION

The utility of the scatterometer for polar remote sensing is its rapid, repeat coverage measurements at a variety of incidence angles, which aid in the separation of ice classes. Backscatter from ice is a function of the measurement incidence angle, θ, and physical properties of the ice. In the incidence angle range $18° \leq \theta \leq 60°$, σ^o (in dB) is approximately a linear function of θ

$$\sigma^o(dB) = \mathcal{A} + \mathcal{B}(\theta - 40°)$$

where the coefficients $\mathcal{A}$ and $\mathcal{B}$ depend on the ice characteristics. $\mathcal{A}$ is the 40° incidence angle-normalized σ^o, while $\mathcal{B}$ describes the dependence of σ^o on θ.

We use the Scatterometer Image Reconstruction (SIR) algorithm to generate enhanced resolution images of $\mathcal{A}$ and $\mathcal{B}$ from the nominally 50 km resolution ERS-1 AMI scatterometer measurements. The SIR algorithm effectively combines multiple passes of the scatterometer over a several day period into a single image with an effective resolution of 30 km [5].

With the aid of the SIR algorithm, a time series of enhanced resolution images of $\mathcal{A}$ and $\mathcal{B}$ have been produced. Each image is based on 6 days of data. These images are input to a simple classification scheme which maps the areal extent of six sea ice types. In this paper we concentrate on the details of separating multiyear ice from pancake ice in the marginal ice zone (MIZ) during the winter months. We also show the time evolution of the sea ice pack over an annual cycle.

II. SEA ICE CLASSIFICATION

Combining multiple measurements of the same location using multiple passes, *Lecomte et al.* [3] used the normalized standard deviation of the normalized difference d between the fore/aft beam measurements,

$$d = |\sigma^o_F - \sigma^o_A| / |\sigma^o_F + \sigma^o_A|,$$

as a measure of the scattering anisotropy in order to distinguish the open ocean from sea ice since sea ice scattering is isotropic while the ocean exhibits a strong azimuthal response.

While most sea ice exhibits an isotropic response [4], the normalized standard deviation can be a useful aid in classifying sea ice surface conditions. For the current application, an image of the normalized standard deviation of the anisotropy is created from the scatterometer measurements taken over the 6 day imaging interval of the SIR algorithm. For each fore-aft measurement pair, the value of d is projected onto a high resolution pixel grid matching the pixel grid used for the SIR images. The aperture weighting need not be used since it factors out and is canceled. The standard deviation of the d values for each pixel is then computed. The result is an image (known as the STD image) that reflects the average anisotropic response of the sea ice surface. Though the resulting image has lower effective resolution than the SIR $\mathcal{A}$ and $\mathcal{B}$ images, this imaging approach results in a somewhat higher resolution than merely binning the data. A sample STD image, where the ocean has been masked off using the detected ice edge, is shown in Fig. 2(a). In this study, we use STD images along with $\mathcal{A}$ and $\mathcal{B}$ images as input to a sea ice classifier.

III. ICE CLASSIFICATION

Drinkwater [1] developed a simple 5 class classifier based on the $\mathcal{A}$ values. A summary of his reported $\mathcal{A}$ values for each class is presented in Table I. The Smooth First Year (SFY), Rough First Year (RFY) and Iceberg classes are distinguishable using $\mathcal{A}$ alone. However, from the $\mathcal{A}$ value alone, it is not possible to distinguish between Multiyear (MY) and MIZ/Pancake (MIZ) ice [1].

The goal of this work is to separate the Multiyear (MY) and MIZ/Pancake (MIZ) classes. Based on scattering characteristics of each ice class, we can predict the behavior of $\mathcal{B}$ and STD for each class. These are summarized in Table II (exact values are not crucial for this discussion).

For simplicity, since all but MY and MIZ ice are separable by $\mathcal{A}$ value, we consider only the $\mathcal{B}$ value and STD values for separating MY ice from MIZ ice. In the algorithm, Pixels are first classified by $\mathcal{A}$ value. A second classification of MY pixels to separate MY and MIZ is then done. Since the $\mathcal{B}$ and STD values for MIZ are higher than for MY ice, we select a threshold for an extended classification algorithm based on the histograms of $\mathcal{B}$ and STD values (see Fig. 1). Using the histograms, the optimum threshold for the $\mathcal{B}$ image data is set at -0.22. The optimum threshold for the STD value is set at

Class	Ice Type	Backscatter Range
ICE	Icebergs	$-6.0 \leq \sigma^o < 0.0$
MY	Multiyear	$-11.0 \leq \sigma^o < -6.0$
MIZ	MIZ/Pancakes	$-11.0 \leq \sigma^o < -6.0$
RFY	Rough First-year	$-14.0 \leq \sigma^o < -11.0$
SFY	Smooth First-year	$-20.0 \leq \sigma^o < -14.0$
NIL	Nilas	$-32.0 \leq \sigma^o < -20.0$

Table I
Summary of winter $\mathcal{A}$ values for each class. Note that multiyear ice and MIZ/pancake ice have the same dB range [1]

0-7803-3836-7/97/$10.00 © 1997 IEEE

Class	Ice Type	$\mathcal{B}$ value	STD value
ICE	Icebergs	Mixed	Mixed
MY	Multiyear	Low	Low
MIZ	MIZ/Pancakes	High	High
RFY	Rough First-year	Mid	Mid
SFY	Smooth First-year	High	Low
NIL	Nilas	High	Low

Table II
Predicted winter $\mathcal{B}$ and STD behavior for each class. MY and MIZ are separable.

0.03. Pixels with $\mathcal{B}$ and STD values above the respective thresholds are classified as MIZ.

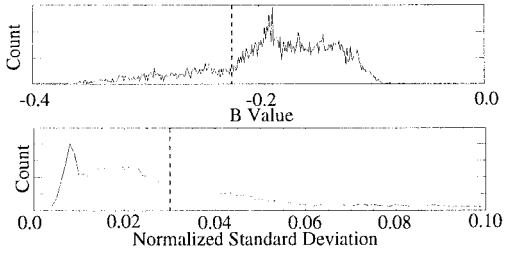

Figure 1. *Histograms of $\mathcal{B}$ and STD values. Vertical lines denote MY/MIZ thresholds.*

IV. VALIDATION

For the Winter Weddell Gyre Study (WWGS) of 1992, the research vessel *Polarstern* was dispatched to enter the sea ice pack and study the surface conditions [2]. During this expedition, a ship borne C-band scatterometer made measurements of the surface conditions of homogeneous ice types, and visual observations of surface conditions were made. This is one of the limited *in situ* observations available for validation of the scatterometer data. Shortly after the ship entered the sea ice pack, a large, persistent field of MIZ/pancake ice was encountered. Later, the ship skirted around a large patch of RFY ice in the middle of the Weddell Sea.

We apply the one-dimensional ($\mathcal{A}$) classifier and use the $\mathcal{B}$ and STD values to separate the MY and MIZ ice classes. Figure 2(b) shows a classified SIR image for JD 168, 1992. While the MIZ region near 0 degrees longitude is classified as MY by $\mathcal{A}$ alone, use of $\mathcal{B}$ and STD correctly classifies this area corresponding to the observed *Polarstern* data. Other regions in and around the sea ice pack have also been classed as MIZ ice, most notably the regions at the ice edge at 45 degrees west and 135 degrees west where we would expect the MIZ because of wave action at the ice edge. Also classed as MIZ are the ice production regions off the Ronne-Filchner ice shelf in the Weddell Sea and the ice production area off the Ross ice shelf.

As validation of the $\mathcal{A}$ algorithm, records from the *Polarstern* show that the ship course was modified to the north to avoid a large mass of rough first-year ice in the center of the Weddell Sea [1, 2]. This feature of the ice pack is clearly represented in the classified SIR image.

While the new algorithm is an improvement over the one-dimensional $\mathcal{A}$ classification, there are indications of some misclassification, e.g., the small amount of MIZ in the typically old ice mass at the tip of the Antarctic Peninsula. Review of images prior to and after this image show that little if any change occurs in the size and shape of this region, confirming the supposition that the area is actually MY ice since MIZ ice tends to rapidly change size and shape as the surface congeals and solidifies into SFY ice. Also, there are small MY areas in the largely MIZ ice class at 0 degrees longitude. However, since previous algorithms classified all MIZ ice, the separation of the majority of pixels in these two classes is considered an important improvement over the one dimensional algorithm.

V. ANNUAL SEA ICE CYCLE 1995

Figure 2(c-f) shows samples from a typical annual cycle of sea ice growth and decay for 1995. These help illustrate the consistency of the classification algorithm.

Figure 2(c) shows an example of the early expansion of the sea ice sheet. A prominent feature is the relatively large quantities of MY ice both in the Weddell Sea and along the continental coast line. In the Weddell Sea, a band of rough first year ice surrounds an inner core of smooth first year ice. This is expected because the ice production begins near the continent, and as the ice ages, deforms and thickens it moves out to make room for newer ice to form off the Ronne-Filchner ice shelf.

Figures 2(d) shows the expanding sea ice pack and the gradual break up of the older ice masses. Notice the substantial reduction in the MY sea ice compared to the first image. Figure 2(e) shows a good example of a typical MIZ ice class near the ice edge at the top of the figure. Figure 2(f) shows the sea ice pack near its maximal extent.

Examination of the full set of images from 1995 shows that the classification results for the various ice classes display a spatial and temporal stability over the course of several annual cycles. The consistency of the ice classes from image to image further supports the definition of the classes while the spatial stability indicates that the classes are useful for studying dynamic motion in the sea ice pack.

VI. SUMMARY

We have extended a simple one dimensional sea ice classifier to separate MIZ/Pancake ice from MY ice in enhanced resolution ERS-1 scatterometer images. The new algorithm uses σ^o at 40° ($\mathcal{A}$), the incidence angle slope of σ^o ($\mathcal{B}$), and the normalized standard deviation of anisotropy (STD) values to distinguish between the two classes.

In situ observations of the sea ice pack made in 1992 were compared with classified imagery to validate the results. The result is a strong correlation between the observed sea ice conditions and the 6 ice classes used. An examination of a full year cycle of sea ice growth and decay in 1995 reveals that the various ice classes show strong spatial and temporal stability from the beginning of the ice pack expansion to the beginning the decay of the sea ice pack. The stability of the classification suggests that the images have value for study of motion in the sea ice pack.

REFERENCES

[1] M.R. Drinkwater, "Satellite Microwave Radar Observations of Antarctic Sea Ice", in *Recent Advances in the Analysis of SAR for Remote Sensing of the Polar Oceans*, C. Tsatsoulis and R. Kwok, Eds. American Geophysical Union, In Press: Submitted October 1996.

[2] M.R. Drinkwater and C. Haas, "Snow, Sea-ice, and Radar Observations During ANT X/4: Summary Data Report," Tech. Rep. 53, Alfred Wegener Institut, July 1994.

[3] P. Lecomte, M. Davison, and A. Cavanie, "Ice Boundary Mapping using ERS-1 Scatterometer Data," *Earth Observation Quarterly*, no. 40, pp. 8, 1993.

[4] D. Early and D.G. Long, "Azimuth Modulation of C-Band Scatterometer σ^o over Southern Ocean Sea Ice," to appear, *IEEE Trans. Geosci. Rem. Sens.*, 1997.

[5] D. Early and D.G. Long, "Enhanced Resolution Imaging from Irregular Samples," *Proc. IGARSS*, Singapore, 1997.

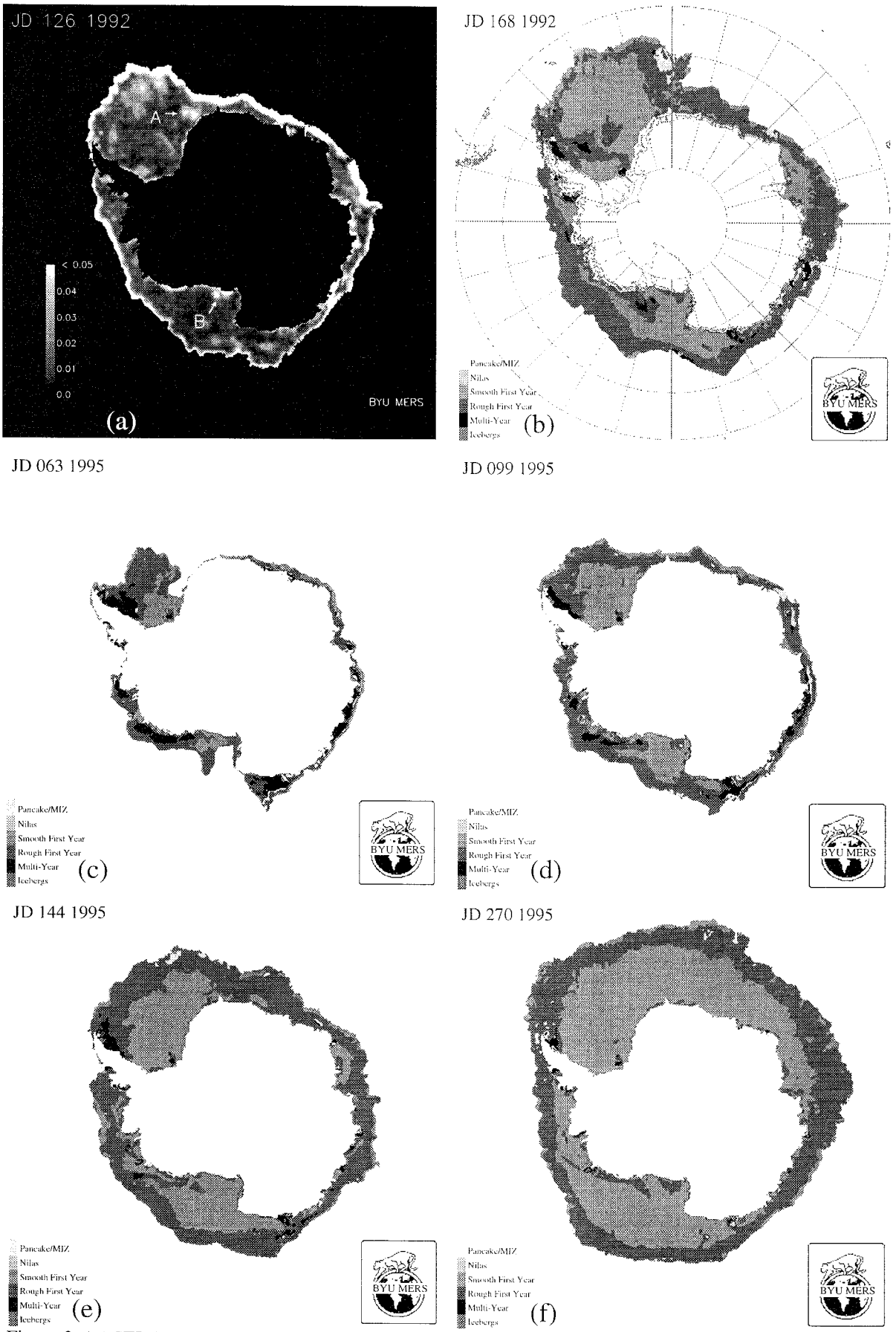

Figure 2. *(a) STD image. Region A warm water upwelling. Region B new ice formation. (b) Classified image 1992. (c-f) time-series of classified images 1995.*